HHS Public Access

Author manuscript

Nucl Med Biol. Author manuscript; available in PMC 2018 March 08.

Published in final edited form as:

Nucl Med Biol. 2013 November ; 40(8): 994–999. doi:10.1016/j.nucmedbio.2013.08.005.

Determining Efficacy of Breast Cancer Therapy by PET Imaging of *HER2* mRNA

Bishnuhari Paudyal[1], **Kaijun Zhang**[1], **Chang-Po Chen**[2], **Matthew E Wampole**[2], **Neil Mehta**[1], **Edith P Mitchell**[3,4], **Brian D Gray**[5], **Jeffrey A Mattis**[5], **Koon Y Pak**[5], **Mathew L Thakur**[1,4], and **Eric Wickstrom**[2,4]

[1]Department of Radiology, Thomas Jefferson University, Philadelphia PA 19107

[2]Department of Biochemistry & Molecular Biology, Thomas Jefferson University, Philadelphia PA 19107

[3]Department of Medical Oncology, Thomas Jefferson University, Philadelphia PA 19107

[4]Department of Kimmel Cancer Center, Thomas Jefferson University, Philadelphia PA 19107

[5]Molecular Targeting Technologies, West Chester PA 19380

Abstract

Introduction—Monitoring the effectiveness of therapy early and accurately continues to be challenging. We hypothesize that determination of Human Epidermal Growth Factor Receptor 2 (*HER2*) mRNA in malignant breast cancer (BC) cells by Positron emission tomography (PET) imaging, before and after treatment, would reflect therapeutic efficacy.

Method—WT4340, a (PNA) *HER2* mRNA was synthesized together with -CSKC, a cyclic peptide, which facilitated internalization of the PNA via IGFR expressed on BC cells, and DOTA that chelated Cu-64. Mice (n=8) with BT474 ER+/*HER2*+ human BC received doxorubicin (DOX, 1.5 mg/kg) i.p. weekly (x3). Mice (n=8) without DOX served as controls. All mice were PET imaged with F-18-FDG and 48 hrs later with Cu-64-WT4340. PET imaging were performed before and 72 hrs after each treatment. Standardized uptake values (SUV) were determined and percent change calculated. Animal body weight (BW) and tumor volume (TV) were measured.

Results—SUV for Cu-64-WT4340 after DOX treatment declined by 54±17% after the second dose, 41±15% after the fourth dose, and 29±7% after the sixth dose compared with 42±22%, 31±18%, and 13±9% ($p<0.05$) for F-18-FDG. In untreated mice, the corresponding percent SUV for Cu-64-WT4340 were 145±82%, 165±39%, and 212±105% of pretreatment SUV compared with 108±28%, 151±8%, and 152±355%, ($p<0.08$) for F-18-FDG. TV in mice after second dose

Corresponding author: Bishnuhari Paudyal, MD, PhD, Department of Radiology, Thomas Jefferson University, 1020 Locust Street, JAH 474, Philadelphia, PA 19107, Tel: +1-215-503-1750, Fax: +1-215-923-9245, bishnuhari.paudyal@jefferson.edu.

Conflict of Interest: B. Paudyal, K. Zhang, C. Chen, N. Mehta, ME. Wampole, EP. Mitchell, BD. Gray, JA Mattis and KY. Pak, have no conflict of interest. MTTI licensed IP from E. Wickstrom/M.L. Thakur.

Some of these data were presented at the Annual Meeting of SNMMI in 2012, Miami, Florida, USA.

were 114.15±61.83 compared with 144.7±64.4% for control mice. BW of DOX-treated mice were 103.4±7.6% of pretreatment, 100.1±4.3 for control mice.

Conclusion—Therapeutic efficacy was apparent sooner by molecular PET imaging than by determination of reduction in TV.

Keywords

copper-64; doxorubicin; peptide nucleic acid; *HER2*; breast cancer

Introduction

Breast cancer (BC) is the most common cancer in women worldwide. In 2013, in the USA alone, over 200,000 new cases of invasive BC will be diagnosed among women, as well as over 50,000 additional cases of in situ BC. Approximately 40,000 women and 500 men are predicted to die from BC in the US in 2013 (1).

Although great strides have been made by chest x-ray, magnetic resonance imaging (MRI) and ultrasound, positron emission tomography (PET) imaging has established itself as the most sensitive modality for monitoring therapy efficacy of malignant lesions (2–6). 2'-F-18-fluorodeoxyglucose (F-18-FDG) PET, which measures glucose utilization in tumors, has been used to determine therapeutic management of different types of cancers. The combined evaluation of morphologic and functional alterations in BC with F-18-FDG PET/CT imaging is considered the most effective means for evaluating therapeutic efficacy for primary and metastatic BC and other cancer (7, 8). Typically however, the effectiveness is measured several weeks after the initiation of treatment.

Early detection of BC gene activity following treatment would provide incremental improvement in BC by reducing the time between the initiation of therapy and to determine its effectiveness. Monitoring the effectiveness of therapy early and accurately continues to be challenging. However, there are no current methods for non-invasively monitoring and quantifying the location, magnitude and extent of gene expression for monitoring therapy. Thus, there is an unmet need to develop a molecular imaging agent that will reveal efficacy of BC treatment early and accurately to manage the disease.

We have designed and demonstrated a novel technology to image cancer gene mRNA based on radionuclide-chelator-peptide nucleic acid (PNA)-peptide agents that specifically imaged *MYCC, CCND1*, and *KRAS2* oncogene mRNAs in tumors (9–12). PNA shows promise as a diagnostic and therapeutic monitoring tool for detecting mRNA expression. PNAs hybridize more strongly and specifically to RNA and DNA than do normal oligonucleotides (13). In addition, PNA resists both proteases and nucleases, does not interact with cellular proteins that normally bind with negatively charged macromolecules, and does not induce RNase degradation of bound mRNA (14).

The Use of Cu-64 ($t_{½}$ 12.7 h, β^+ 17.4%, β^- 41%) has been gaining increased interest in the field of targeted PET imaging and therapy due to its both β^+ and β^- emission (4, 5, 15).

Imaging of cancer gene expression with Cu-64-PNA approach enables investigators to choose appropriate molecular intervention at the onset of the disease.

We hypothesized that monitoring Human Epidermal Growth Factor Receptor 2 (*HER2*) mRNA expression before and within less than a week after the initiation of treatment would determine treatment effectiveness or resistance sooner than computerized tomography (CT) or MR imaging. To test our hypothesis that quantification of *HER2* mRNA in malignant BC by PET imaging would reflect therapeutic efficacy, we report herein imaging results in immunocompromised mice carrying human BT474 BC xenografts before and after doxorubicin (DOX) therapy.

Materials and Methods

Design and Synthesis of DOTA-PNA-Peptide mRNA Imaging Agents

The preparation of [Cu-64] 1,4,7,10-tetraazadodecane-N,N',N'',N'''-tetraacetic acid (DOTA)-*HER2*-PNA-IGF1 hybridization agents is illustrated in Scheme 1, as described for *CCND1* mRNA PET imaging (11). The hybridization agents composed of four fragments: (I) D-tetrapeptide cyclized with a Cys-Cys disulfide bridge to enable receptor-mediated endocytosis of PNA agents for cell-type specific delivery; (II) a PNA sequence targeting the start codon region of an overexpressed oncogene mRNA, because the start codon region is usually available for PNA hybridization; (III) a DOTA chelator that strongly binds a positron-emitting radionuclide; (IV) hydrophilic 8-amino-3,6-dioxaoctanoic acid aminoethoxyethoxyacetate (AEEA) spacers in between DOTA/PNA, PNA/peptide fragments to increase the flexibility of the targeting ligand and imaging ligand, which will enhance the hybridization efficiency of PNA.

The synthesis of DOTA-*HER2* PNA-IGF1 analog (WT4340) was carried out continuously on NovaSyn Sieber resin (0.2 mmol/g, Novabiochem) on a 20 μmol scale using standard solid phase Fmoc coupling activated by 2-(7–aza-1H-benzotriazole-1-yl)-1,1,3,3-tetramethyl-uronium-hexafluorophosphate (HATU) on an PS3 peptide synthesizer (Protein Technologies, Inc.). Two control sequences were synthesized (Scheme 1), one (WT4314) with a mismatched base to minimize hybridization to *HER2* mRNA, and another (WT4289) with a mismatched amino acid residue that does not enable IGF1R-mediated uptake. The cysteine residues were cyclized on the solid phase with 10 equivalents of I_2 in $(CH_3)_2NCHO$ for 4 h at room temperature. Next, the resin was washed with $(CH_3)_2NCHO$ and MeOH and dried under vacuum, then cleaved and deprotected with CF_3CO_2H/m-cresol/i-Pr_3SiH (90:8:2) for 4 h at room temperature. After removal of the resin by filtration, the filtrate was added to cold EtOEt to precipitate the conjugates as off white solid products.

The agents were purified by reversed phase high-performance liquid chromatography (HPLC) on an Alltech Alltima C_{18} column (5 μm particle size, 10 × 250 mm) (Grace) eluted with a linear gradient of 5–55% CH_3CN in aqueous 0.1% CF_3CO_2H over 30 min at 50°C at a flow rate of 4 mL/min by a 600F pump (Waters), monitored by absorbance at 260 nm on a 486 detector (Waters). The major peaks were collected, then concentrated, and lyophilized. Products were analyzed by HPLC on an Altima C_{18} column (5 μm particle size, 4.6 × 250 mm) eluted with a linear gradient of 5–55% CH_3CN in aqueous 0.1% CF_3CO_2H over 30

min at 50°C at a flow rate of 0.5 mL/min, monitored by absorbance at 260 nm. Product peaks were characterized by mass spectroscopy (MS) on a 4800 MALDI TOF/TOF Analyzer (Applied Biosystems).

Preparation of Cu-64 PNA-Peptide Radiohybridization Agents

The DOTA-PNA-peptides were labeled with Cu-64 (Scheme 1) as previously described (11). In brief, 20 μg (~ 4.5 nmol) of PNA-peptides were dissolved in 20 μL of sterile water. Then, 2 μL of Cu-64Cl2 (7.4–11.1 MBq [200–300 μCi], ~ 1 nmol) (specific activity ~ 300 Ci/mmol) in 0.1 M HCl (Washington University, St. Louis, MO) were added. Finally, 200 μL of 0.1 M NH_4OAc, pH 5.5, were added to the solution, which was then incubated at 90°C for 15 min.

Quality Control

The radiochemical purity of the Cu-64-PNA-peptides was monitored by reverse-phase HPLC on a Dynamax C_{18} column (300-Å pore, 5-μm particle size, 4.5 × 250 mm; Varian, Inc.) eluted at 1 mL/min with aqueous 0.1% CF_3CO_2H in a gradient from 10% to 100% CH_3CN over 40 min at 25°C on a Shimadzu (Kyoto, Japan) HPLC coupled to a UV detector, NaI (Tl) radioactivity monitor, and a rate meter. Cu-64-PNA-peptide labeling yields were 95%–99%. Cu-64-PNA-peptide retention time was 12.0 min. The thermodynamic stability of Cu-64-PNA-peptide over time was determined by HPLC by incubation with 100-fold molar excesses of DTPA, human serum albumin, or cysteine at 22°C for 30 min as described (11). A control sequence, the *CCND1*-specific [^{64}Cu] DOTA-PNA-IGF1 analog WT4348, was administered to a mouse to test for probe stability in circulating blood. Serum prepared from a blood draw 3 min. after administration was analyzed by SDS-PAGE and autoradiography as previously described (11). Scintillation counting of excised bands revealed that approximately 50% of Cu-64 component had the same molecular weight as WT4348 (4–5 kD). The radiochemical purity of Cu-64-PNA-peptides was consistent throughout the experiments.

Human BT474 BC Cell Culture

Estrogen receptor-positive, Her2 + BT474 BC cells (American Type Culture Collection) were maintained in RPMI 1640 medium with 2 mM L-glutamine, 1.0 mM sodium pyruvate, 1.5 g/L sodium bicarbonate, 4.5 g/L glucose, 0.2 Units/ml bovine insulin, 50 U/mL penicillin, 5 μg/mL streptomycin, (90 %) and fetal bovine serum (10%) at 37°C under 5% CO_2 and 95% air. The cells when confluent were detached using 0.25% trypsin-EDTA, washed and resuspended with RPMI-1640 medium at a concentration of approximately 25 $\times 10^6$ cells/ml.

BT474 Cell Binding of [Cu-64] DOTA-*HER2* PNA-IGF1 Tetrapeptides

Her2+ BT474 breast cancer cells express thousands of *HER2* mRNA per cell, resulting in high levels of Her2 protein on the cell surface. For uptake of Cu-64-WT4340, cells were detached from their flasks in the absence of trypsin, with 0.02% EDTA solution (Sigma). Aliquots of $10.0 \pm 1.0 \times 10^6$ cells were dispensed in 0.5 mL of culture medium in test tubes. To each tube 2.8 pmol (1.66×10^{12} molecules) of Cu-64-WT4340 in 0.1 M NH_4OAc, pH 5.5,

were added, mixed, and incubated at 22°C for 30 min. Cells were then sedimented at 450 g for 5 min, and the supernatants were saved for counting. Cells were then washed twice with RPMI 1640. The three supernatants were combined. Radioactivity associated with the supernatants and with the cell pellets was determined.

Human BT474 BC Xenografts

For tumor induction, 5–6 × 10^6 BT474 cells in 0.2 mL of culture medium, including 10 mg of Matrigel (Becton-Dickinson), were implanted intramuscularly through a sterile 27 gauge needle into the thighs of 6–8 week old female NCr immunocompromised mice (National Cancer Institute), lightly anesthetized with a mixture of ketamine (200 mg/kg), xylazine (10 mg/kg) and acetopromazine (2 mg/kg) at a dose of 160 μL/25 g, as before (11). Animals were examined regularly for the presence of tumors. Mice bearing tumors with ≥5 mm diameter were entered into the study. At the end of the experiment, animals were euthanized in a halothane chamber, consistent with USDA regulations and American Veterinary Medical Association recommendations. Animal experiments were conducted in accordance with institutional guidelines. Protocols (no. 118FF) were approved in advance by the Institutional Animal Care and Use Committee of Thomas Jefferson University. Animals were weighed twice a week in calibrated digital balances and TV was measured using a digital vernier caliper. Three readings were obtained on each tumor and averaged. The first week TV and BW before treatment were considered to be 100%. The post-treatment values are presented as a percentage of the 1^{st} week pretreatment TV or BW.

PET/CT

Animals were fasted for 4 h before the administration of F-18-FDG (178 ± 27 μCi) via a lateral tail vein. Animals were anesthetized with an intraperitoneal injection of a mixture of ketamine (200 mg/kg), xylazine (10 mg/kg), and acetopromazine (2 mg/kg) at a dose of 160 μL/25 g, as described (11) only for F-18-FDG PET imaging to minimize the unwanted muscle uptake. Animals were kept under 1.5% isoflurane and 98.5% O_2 during the radioactive uptake and scan period. PET/CT imaging was performed at 1 h after the injection of F-18-FDG. Cu-64-WT4340 (128± 34 μCi) in 0.1 M NH_4OAc, pH 5.5, was administered 48 h after the F-18-FDG study (26 half-lives). PET/CT imaging was performed at 4 h and 24 h after the injection of Cu-64-WT4340. CT was performed first, followed by PET for both studies.

PET imaging was performed using an Inveon small animal PET scanner (Siemens, Knoxville TN, USA) which has high spatial resolution (1 mm in full width at half maximum) and sensitivity, as described (15). An ordered-subset expectation maximization 3-dimensional (3D) algorithm with 5 iterations and 8 subsets was used for reconstruction. PET imaging of each mouse was followed by noncontrast CT using a MicroCAT II CT scanner (ImTek Inc.; Siemens), yielding reconstructed voxels of 103 × 103 × 103 μm. A Feldkamp, Davis, and Kress cone-beam algorithm was used for reconstruction. 3D visualization software provided high-quality images including surface-rendered and maximum-intensity-projection images.

Image Processing and Quantification

An Inveon Research Workstation (Siemens) was used for image processing and analysis. An automatic rigid registration algorithm with weighted mutual information as a measure of similarity was used for registering PET and CT datasets as described (15). The anatomic location of the tumor was identified from the registered datasets. Volumes of interest (VOIs) were created on the tumor PET images, and standardized uptake values (SUVs) for dose and body weight were calculated using Inveon Research Workplace 3.0, Analysis Application, Ed 3.0.0.55 (Siemens USA). The first week SUV measurements before treatment were considered to be 100%. Post-treatment SUVs (3^{rd} week, 5^{th} week and 7^{th} week) were expressed as a percentage of the 1^{st} week pretreatment SUV for comparison.

The PET scanner was calibrated with known activity to get the SUV for body weight values from the VOI. Amira 5 (Visage Imaging Inc.) was used for 3D visualization. PET and CT datasets were registered in Amira using a rigid registration algorithm with normalized mutual information as the measure of similarity. Surface rendering was performed using the threshold pixel value for bone from the CT dataset and the tumor from the PET dataset to localize the tumor with reference to the skeleton.

Statistical analysis

Data were expressed as mean±standard deviation. Means were compared using Student's t-test. *P* values of less than 0.05 were considered statistically significant.

Results

Synthesis Cu-64 labeling and cell binding of DOTA-HER2 PNA-IGF1 analogs

The molecular masses of the Cu-64-*HER2* PNA-peptides used are given in Table 1.

Cu-64 labeling of WT4340 was measured by C_{18} reversed phase chromatography (Fig. 1), indicating a yield of 97.5%. Following incubation with BT474 cells, Cu-64 radioactivity associated with cells on the plate vs. that remaining in the supernatants was determined (Table 2). The BT474 cells showed 3-fold greater accumulation of the antisense Cu-64-WT4340 than of either mismatch control agent, within experimental error. Thus, the antisense Cu-64-WT4340 displayed significant specificity to proceed with animal imaging using only WT4340. Earlier animal imaging studies of *CCND1, MYCC,* and *KRAS2* mRNAs in xenografts yielded only background signals with mismatch agents or control xenografts (9–12).

PET/CT imaging of BT474 xenografts with and without DOX therapy

Three-dimensional PET/CT fusion of a representative BT474 xenograft, imaged by Cu-64-WT4340 or by F-18-FDG (Fig. 2) showed diminished avidity after two doses of DOX, but prominent contralateral muscle uptake. With Cu-64-WT4340 PET imaging, contralateral muscle uptake was negligible. In our previous study of *CCND1* mRNA PET imaging with the same kind of Cu-64-PNA-IGF1 tetrapeptide agent, IGF1 receptor blocking with recombinant IGF1 successfully blocked tumor uptake as much as a PNA mismatch, or a

peptide mismatch (11). Since our *HER2* agent relies on the same IGF1 receptor utilized in the *CCND1* study, we are confident that agent uptake is receptor-dependent.

SUV calculations for the entire cohort of 8 DOX-treated mice and 8 untreated mice are shown in Fig. 3. Compared with pretreatment values, the first week SUV measurements before treatment were considered to be 100%. Post-treatment SUVs (3rd week, 5th week and 7th week) were expressed as a percentage of the 1st week pretreatment SUV for comparison. SUV for Cu-64-WT4340 after DOX treatment declined by 54±17% after the second dose, 41±15% after the fourth dose, and 29±7% after the sixth dose, compared with 42±22%, 31±18%, and 13±9%, ($p<0.05$) for F-18-FDG. In untreated mice, the corresponding % SUV for Cu-64-WT4340 were 145±82%, 165±39%, and 212±105% of pretreatment SUV, compared with 108±28%, 151±8%, and 152±355%, ($p<0.08$) for F-18-FDG.

TV of treated mice were decreased and untreated control mice were increased however, BW of DOX-treated mice were not dramatically change rather remained constant, compared with untreated mice (Table 3). The TV in mice after the second treatment were 114.15±61.83%, after the fourth treatment 105.9±59.6%, and after the sixth treatment 80.36±46.5% compared with 144.7±64.4%, 162.7±80.5%, and 213.2±77.7% for control mice. The BW of DOX-treated mice were after the second treatment 103.4±7.6% after the fourth treatment, 107.9±6.2% and after the sixth treatment, and 102.9±5.8% compared with 100.1±4.31%, 102.6±5.7%, and 102.7±7.4% for control mice.

Discussion

The present study demonstrated that mRNA PET imaging with the Cu-64-*HER2* PNA-IGF1 tetrapeptide agent WT4340 could be utilized for the imaging of BC gene expression. Such agents remain intact in circulating mouse blood.

The current study indicates that declining SUV occurs earlier than declining tumor volume. Data also indicate that Thus, therapeutic efficacy was apparent sooner by molecular PET than by determination of reduction in TV. mRNA PET imaging permits assessment of the metabolic and genomic activity earlier than tumor volume and weight change. The present finding is consistent with a previous report that changes in metabolic activity generally occur earlier than changes in tumor size (2), which is the current standard for the assessment of a response. However, no technique exists that provides correct assessment of down-regulated oncogenic mRNA resulting from therapeutic intervention. The degree of changes in F-18-FDG uptake and Cu-64-WT4340 after the initiation of therapy is correlated with the histopathologic response after the completion of therapy.

Our previous study using the *CCND1* agent Cu-64-WT4348 demonstrated receptor specific tumor uptake of the PNA agent (11). Earlier Ross et al. demonstrated the potential usefulness of *HER2* in the prediction of response to hormonal, cytotoxic, and radiation therapies in BC patients (16). Similarly, recombinant humanized anti-Her2 monoclonal antibody, trastuzumab, administered as a single agent, produces durable objective responses and is well tolerated by women with Her2-overexpressing metastatic breast cancer that has progressed after chemotherapy (17) and in combination with chemotherapy (18).

Completion of adjuvant chemotherapy provides useful information concerning the efficacy of treatment and the prognosis of patients with breast cancer (19, 20). Cu-64-DOTA-trastuzumab appears to be effective as a PET tracer for imaging Her2/neu in lung cancer (5). Thus, the use of *HER2* mRNA as the target is justified in radiohybridization detection and in monitoring the effectiveness of therapy in Her2+ breast cancer patients.

The insulin-like growth factor 1/insulin like growth factor 1 receptor (IGF1/IGF1R) system plays a major regulatory role in development, cell cycle progression, and the early phase of tumorigenicity (21). Neoplastic transformation is often related to abnormal activation of growth factor receptors and their signaling pathways. Experimental and clinical data strongly suggest that IGF1R is involved in breast cancer development and progression. Activation of IGF1R has been shown to impede the efficacy of standard breast cancer herapeutics, as well as compounds targeting other oncogenic receptors, such as Her2 (22, 23).

Consistent with our hypothesis, the present study indicated that Cu-64-WT4340 PET imaging of mRNA expression, non-invasively, could provide a more useful therapy monitoring tool than the currently available modalities. None of the current modalities can image oncogene mRNA expression directly, nor monitor the effectiveness of therapy. Therefore, present findings might help to improve the accuracy of monitoring therapeutic activity, demonstrate better evidence for non-responsive therapy, and guide substitution with an alternative regimen.

Acknowledgements

This work was supported by NIH 1R44CA136306. MTTI licensed IP from E. Wickstrom/M.L. Thakur.

References

1. American Cancer Society Breast Cancer Facts & Figures. 2012
2. Avril N, Sassen S, Roylance R. Response to therapy in breast cancer. J Nucl Med. 2009; 1:55S–63S.
3. Hanaoka H, Katagiri T, Fukukawa C, et al. Radioimmunotherapy of solid tumors targeting a cellsurface protein, FZD10: therapeutic efficacy largely depends on radiosensitivity. Ann Nucl Med. 2009; 5:479–485.
4. Paudyal B, Paudyal P, Oriuchi N, Hanaoka, et al. Positron emission tomography imaging and biodistribution of vascular endothelial growth factor with Cu-64-labeled bevacizumab in colorectal cancer xenografts. Cancer Sci. 2011; 102:117–121. [PubMed: 21070475]
5. Paudyal P, Paudyal B, Hanaoka H, et al. Imaging and biodistribution of Her2/neu expression in non-small cell lung cancer xenografts with Cu-labeled trastuzumab PET. Cancer Sci. 2010; 101:1045–1050. [PubMed: 20219072]
6. Wu CY, Chou LS, Chan PC, et al. Monitoring tumor response with radiolabeled nucleoside analogs in a hepatoma-bearing mouse model early after Doxisome (®) treatment. Mol Imaging Biol. 2013; 15:326–335. [PubMed: 23247923]
7. Schwarz JK, Grigsby PW, Dehdashti F, et al. The role of F-18-FDG PET in assessing therapy response in cancer of the cervix and ovaries. J Nucl Med. 2009; 50:64S–73S. [PubMed: 19380409]
8. Tomasi G, Rosso L. PET imaging: implications for the future of therapy monitoring with PET/CT in oncology. Curr Opin Pharmacol. 2009; 12:569–575. 2012.
9. Tian X, Aruva MR, Qin W, et al. External imaging of CCND1 cancer gene activity in experimental human breast cancer xenografts with ^{99m}Tc-peptide nucleic acid-peptide chimeras. J Nucl Med. 2004; 45:2070–2082. [PubMed: 15585484]

10. Tian X, Aruva MR, Qin W, Zhu W, Sauter ER, Thakur ML, Wickstrom E. Noninvasive molecular imaging of MYC mRNA expression in human breast cancer xenografts with a [^{99m}Tc] peptide-peptide nucleic acid-peptide chimera. Bioconj Chem. 2005; 16:70–79.
11. Tian X, Aruva MR, Zhang K, et al. PET imaging of CCND1 mRNA in human MCF7 estrogen receptor-positive breast cancer xenografts with an oncogene specific [Cu-64] DO3APNA-peptide radiohybridization probe. J Nucl Med. 2007; 48:1699–1707. [PubMed: 17909257]
12. Amirkhanov NV, Zhang K, Aruva MR, et al. Imaging human pancreatic cancer xenografts by targeting mutant KRAS2 mRNA with [(^{111})In]DOTA(n)-poly(diamidopropanoyl)(m)-KRAS2 PNA-D(Cys-Ser-Lys-Cys) nanoparticles. Bioconjug Chem. 2010; 21:731–740. [PubMed: 20232877]
13. Egholm M, Buchardt O, Christensen L, et al. PNA hybridizes to complementary oligonucleotides obeying the Watson-Crick hydrogen-bonding rules. Nature. 1993; 365:566–568. [PubMed: 7692304]
14. Good L, Nielsen PE. Progress in developing PNA as a gene-targeted drug. Antisense Nucleic Acid Drug Dev. 1997; 7:431–437. [PubMed: 9303195]
15. Thakur ML, Devadhas D, Zhang K, et al. Imaging spontaneous MMTVneu transgenic murine mammary tumors: targeting metabolic activity versus genetic products. J Nucl Med. 2010; 51:106–111. [PubMed: 20008985]
16. Ross JS, Fletcher JA. The HER-2/neu Oncogene in Breast Cancer: Prognostic Factor, Predictive Factor, and Target for Therapy. Oncologist. 1998; 3:237–252. [PubMed: 10388110]
17. Cobleigh MA, Vogel CL, Tripathy NJ, et al. Multinational study of the efficacy and safety of humanized anti-Her2 monoclonal antibody in women who have Her2-overexpressing metastatic breast cancer that has progressed after chemotherapy for metastatic disease. J Clin Oncol. 1999; 17:2639–2648. [PubMed: 10561337]
18. Slamon D, Leyland-Jones B, Shak S, et al. Use of chemotherapy plus a monoclonal antibody against Her2 for metastatic breast cancer that overexpresses Her2. N Engl J Med. 2001; 344:783–792. [PubMed: 11248153]
19. Bertram J, Killian M, Brysch W, et al. Reduction of erbB2 gene product in mamma carcinoma cell lines by erbB2 mRNA-specific and tyrosine kinase consensus phosphorothioate antisense oligonucleotides. Biochem Biophys Res Commun. 1994; 200:661–667. [PubMed: 7909438]
20. Vaughn JP, Stekler J, Demirdji S, et al. Inhibition of the erbB-2 tyrosine kinase receptor in breast cancer cells by phosphoromonothioate and phosphorodithioate antisense oligonucleotides. Nucleic Acids Res. 1996; 24:4558–4564. [PubMed: 8948649]
21. Muller WJ, Arteaga CL, Muthuswamy SK, et al. Synergistic interaction of the Neu protooncogene product and transforming growth factor alpha in the mammary epithelium of transgenic mice. Mol Cell Biol. 1996; 16:5726–5736. [PubMed: 8816486]
22. Surmacz E. Function of the IGF-I receptor in breast cancer. J Mammary Gland Biol Neoplasia. 2000; 5:95–105. [PubMed: 10791772]
23. Pollak M. IGF-I physiology and breast cancer. Recent Results Cancer Res. 1998; 152:63–70. [PubMed: 9928547]

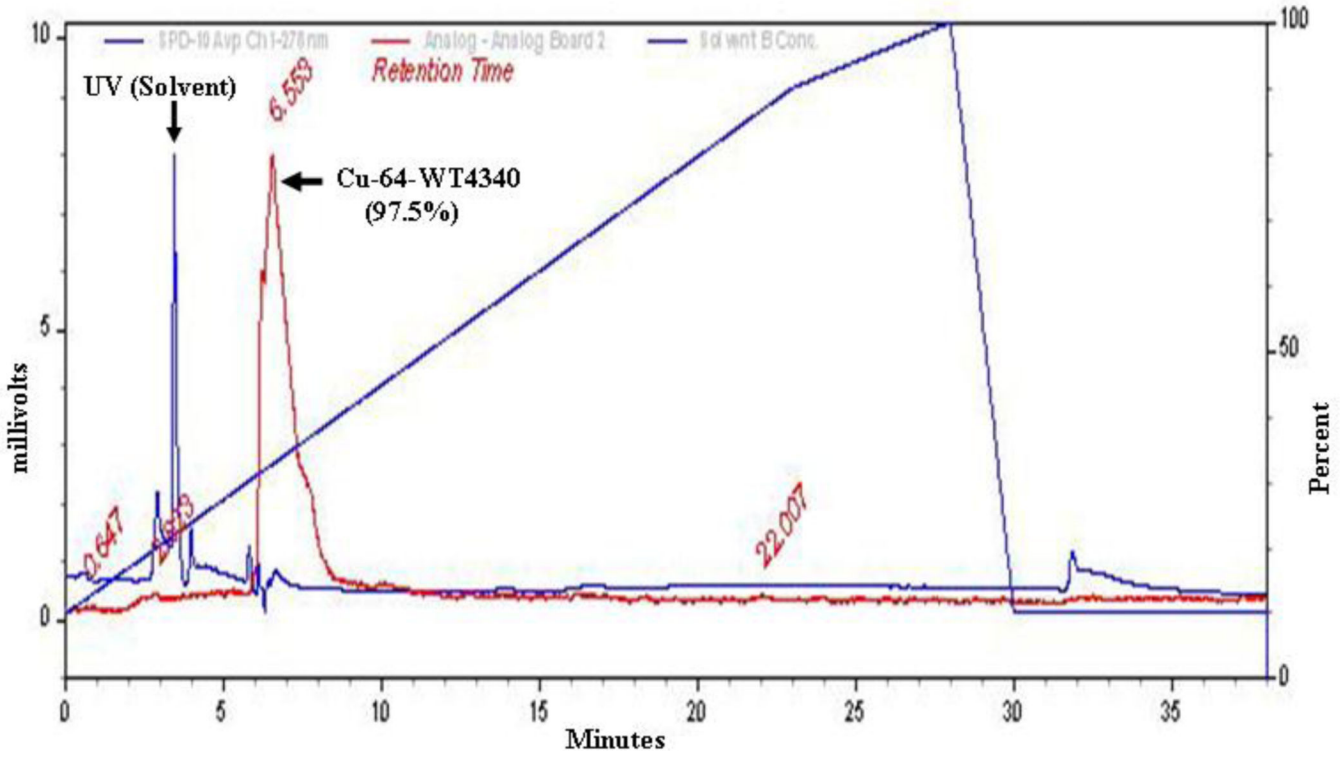

Figure 1.

HPLC elution curve of Cu-64-WT4340 shows (arrow) more than 97.5% Cu-64 is associated with a peak at 6.5 min and only minimal free Cu-64 at 2.9 min. Diagonal line represents gradient.

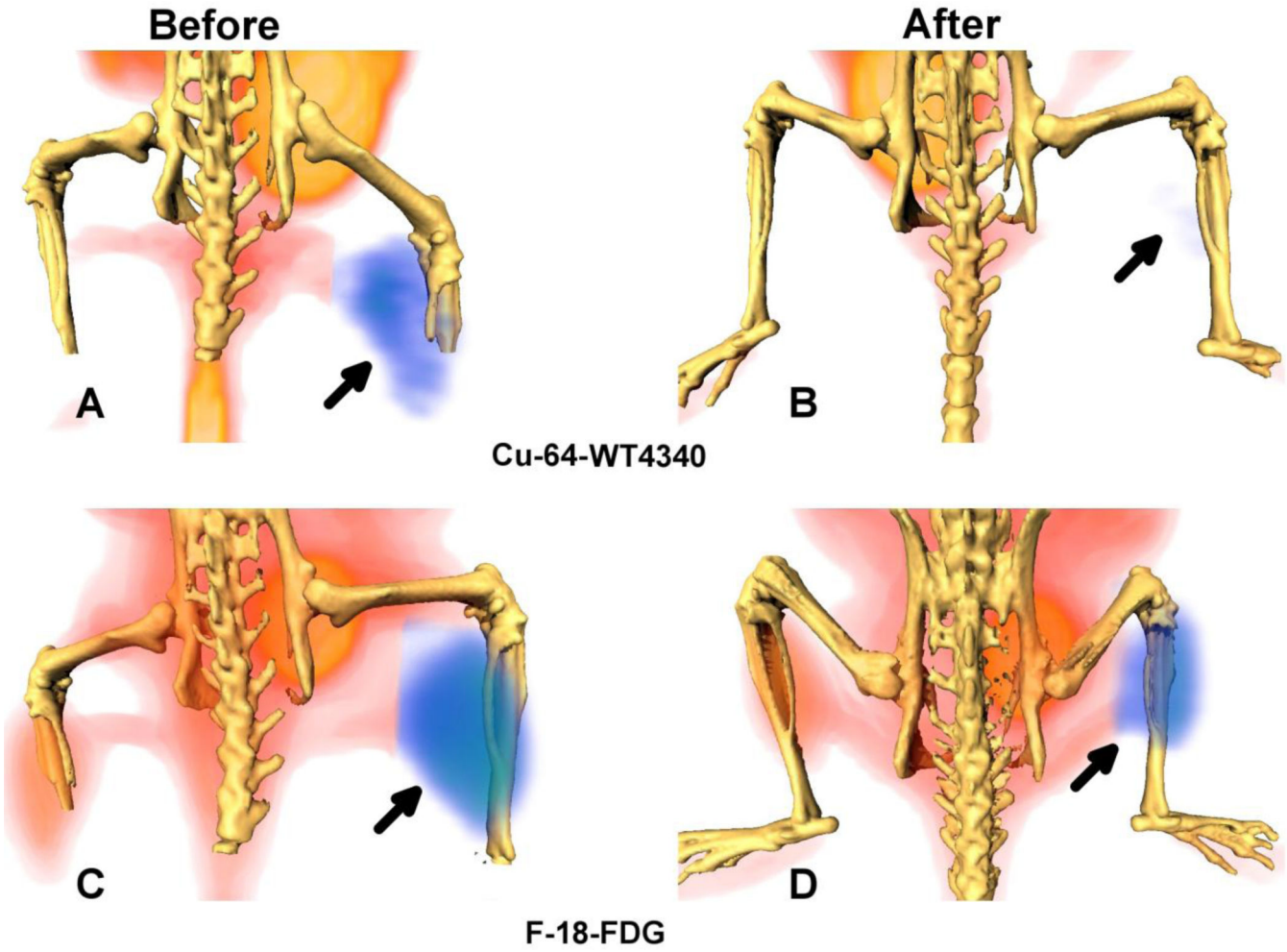

Figure 2.

Surface rendered F-18-FDG and Cu-64-WT4340 images of a mouse bearing BT474 tumor (arrow) in the right thigh. Images in A and C are before treatment and in B and D are after second Dox treatment. Top: Cu-64-WT4340 (A, B) Bottom: F-18-FDG (C, D). A significantly diminished uptake of Cu-64-WT4340 after Dox treatment is visible in (B) as compared to that with the F-18-FDG uptake (D). Note: significant muscle uptake of F-18-FDG in contralateral normal thigh (C).

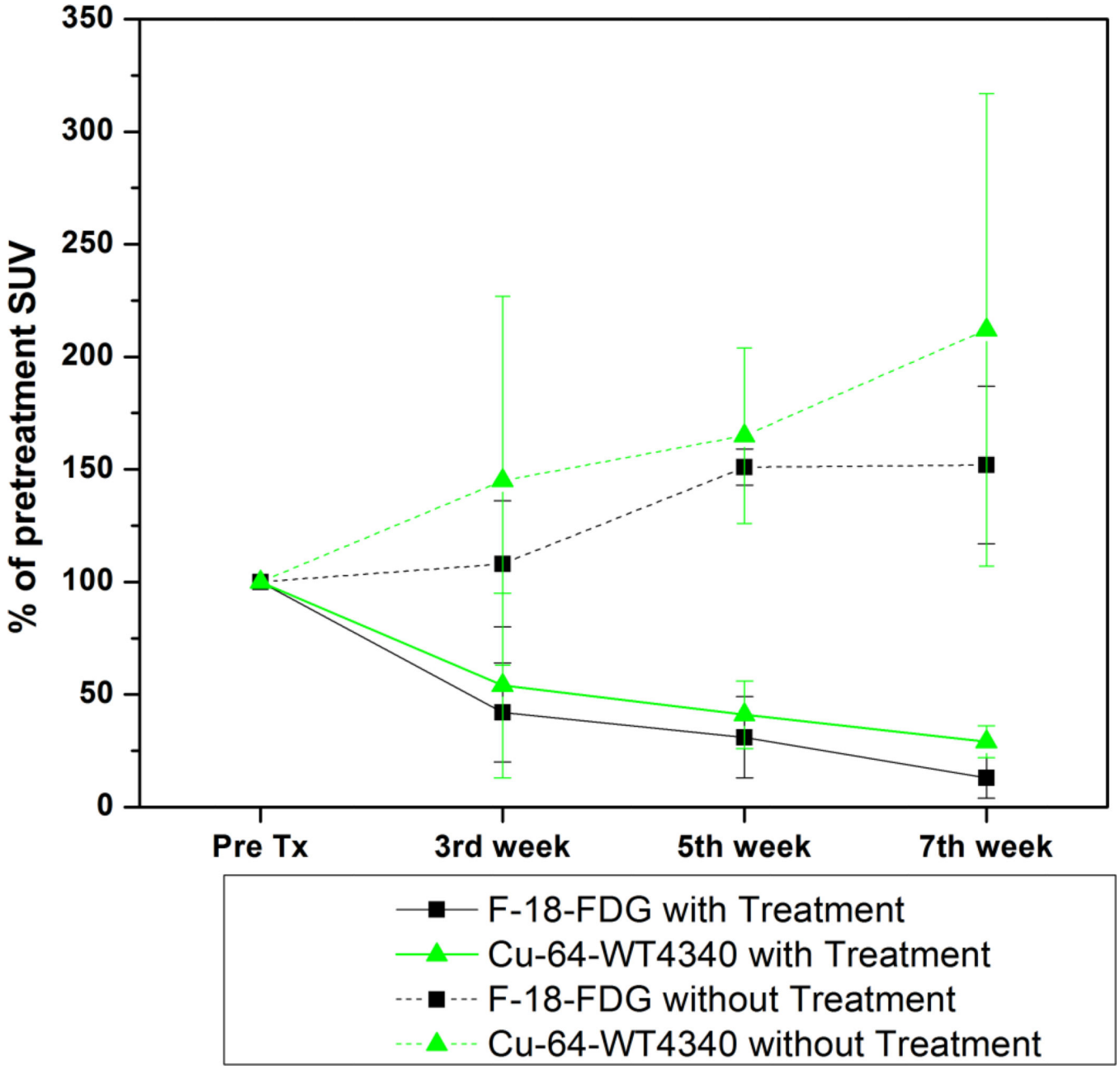

Figure 3.

SUV in each tumor was determined and presented as the percentage of the SUV prior to treatment in each mouse. The first week SUVs before treatment were considered to be 100%. Post-treatment SUVs (3^{rd} week, 5^{th} week and 7^{th} week) were expressed as a percentage of the 1st week pretreatment SUV for comparison.

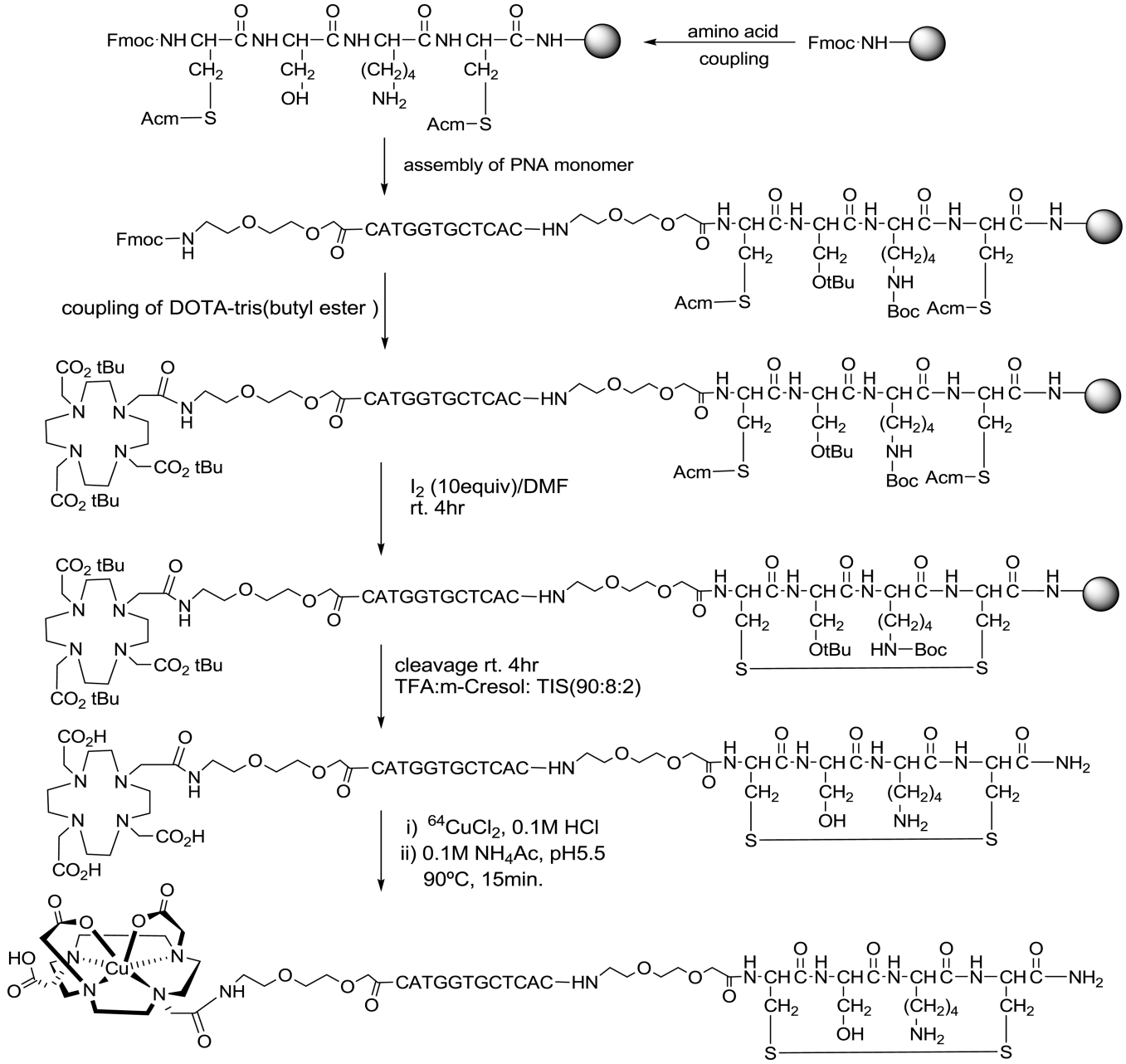

Scheme 1.

Synthesis of [Cu-64]DOTA-HER2-PNA-IGF1 tetrapeptide hybridization agents (WT4340)

Table 1

Retention times and molecular masses of DOTA-PNA-peptides

Target	Agent	Retention (min)[a]	Mass, Da (calc.)	Mass, Da (found)[b]
HER2 antisense	WT4340	23.6	4338.75	4339.52 (+1)
PNA mismatch	WT4314	24.1	4313.74	4314.70 (+1)
Peptide mismatch	WT4289	22.4	4284.23	4285.85 (+1)

[a] C18 reversed phase chromatography.

[b] MALDI-TOF spectroscopy

Table 2

DOTA-PNA-Peptide Cu-64 radiolabeling and BT474 Cellular Uptake

Target	HER2 Antisense	PNA Mismatch	Peptide Mismatch
Agent	WT4340	WT4314	WT4289
Cu-64 radiochemical purity[a]	98.80%	94.90%	98.30%
BT474 cell uptake[b]	17.78%	8.84%	8.80%
	25.49%	8.71%	9.13%
	25.66%	7.18%	9.43%
Mean value	22.98±4.50%	8.24±0.92%	9.12±0.32%
Null probability		p<0.01	p<0.01

[a] C18 reversed phase chromatography.

[b] scintillation counting of cell pellets

Table 3

Percent of Pretreatment Tumor Volume (TV) and Body Weight (BW) of mice bearing BT474 Xenografts with and without (n=8) Doxorubicin Treatment (n=8)

Pre-treatment measures		Post treatment percentages		
Variables	**Week 1[a]**	**Week 3[b]**	**Week 5[b]**	**Week 7[b]**
Treated mouse weight	100% (23.46±2.2 g)	103.4±7.6%	107.9 ±6.2%	102.9±5.8%
Treated tumor volume	100% (24.35±2.7 mm^3)	114.2±61.8%	105.9±59.6%	80.36±46.5%
Control mouse weight	100% (25.25±4.3 g)	100.1±4.3%	102.6±5.7%	102.7±7.4%
Control tumor volume	100% (24.35±3.4 mm^3)	144.7±64.4%	162.7±80.5%	213.2±77.7%

[a] first week TV and BW before treatment were considered to be 100%, relative to post-treatment values.

[b] percentage of 1st week pretreatment TV or BW